17th AIAA/CEAS Aeroacoustics Conference (32nd AIAA Aeroacoustics Conference)
05 - 08 June 2011, Portland, Oregon

AIAA 2011-2799

On the Development and Application of a Hybrid Approach to the Simulation of Broadband Noise in a Lobed Mixer

Jens Wellner* and Thomas Röber*

German Aerospace Center, Cologne, 51147, Germany

Paul Traub§

MTU Aero Engines GmbH, Munich, 80995, Germany

This study is focused on developing a process that couples the near-field unsteady flow field data computed by a 3-D Detached Eddy Simulation (DES) code with a Ffowcs Williams - Hawkings (FW-H) formulation for the far-field noise prediction of turbulent jets. In particular the numerical method to create a general and flexible interface between these simulation methodologies is presented. It is shown that using DES for the near-field and a FW-H approach for the far-field yields a versatile tool for jet noise prediction.

Nomenclature

c_0	speed of sound
c_b	bias constant of DES scheme
C_{DES}	calibration constant of DES model ($C_{\mathrm{DES}} \approx 0.1$)
D_f	convective amplification factor
f	frequency
l	turbulence length scale
$l_{k\omega}$	turbulence length scale by RANS model
k	free-field wave number
p	pressure
r_0	nozzle radius
R_e	emission distance
t	time
$\mathbf{u}$	velocity vector
$\mathbf{x}$	observer position
$\mathbf{y}$	position on the permeable surface
Subscripts/Superscripts	
0	steady ambient condition
$1, 2, 3$	indices for Cartesian coordinates
i, j	Einstein notations
i, j, k	numerical indices
$()'$	time domain fluctuation
Greek symbols	
β	turbulence model closure coefficient $\beta = 0.09$
ϵ	specific turbulent dissipation
Γ_{1i}	spatial derivative of the emission distance
Γ_{2i}	spatial derivative of product $R_e D_f$
κ	parameter of MUSCL scheme
ρ	air density
ϕ	transported quantity
o_{DES}	DES blending function
τ	retarded time
τ_{ij}	viscous stress tensor
Δ	mesh length scale (DES filter width)
ω	angular frequency

I. Introduction

The flow in mixer nozzles is characterized by shear layers with strong velocity gradients between bypass and core flow, giving rise to strong turbulent structures in both circumferential and radial directions, which interact with the tonal noise field from the turbomachinery parts on the one hand and cause broadband noise on the other. In this paper, the results of a Detached Eddy Simulation (DES) of the flow through a lobed mixer and the region immediately downstream (ca. 5 nozzle diameters behind the nozzle exit) are

*Research Engineer, German Aerospace Center, Institute of Propulsion Technology, Linder Höhe, 51147 Cologne.
§Physicist, MTU Aero Engines GmbH, Aerodynamics, Aeroelasticity, Aeroacoustics Turbine (TEAT), P.O.Box 50 06 40, 80976 Munich, Germany.

presented. The particular geometry of lobed mixers intertwines core and bypass flow, so that a complicated flow pattern emerges.
In modern aircraft engines, the exhaust jet is one of the major contributors to engine noise, especially at full throttle conditions, e.g. during take-off. Therefore, current mixer nozzles are designed to provide efficient mixing between core and bypass flows while keeping noise levels low. This usually leads to rather complicated shapes of mixer geometries, and thus to complicated flow patterns.
In noise calculations, one can separate the computation into two parts: in the first part, the nonlinear generation of sound is obtained using techniques such as Direct Numerical Simulation (DNS), Large Eddy Simulation (LES) or Detached Eddy Simulation (DES); in the second part, the sound propagation to the far field is calculated. This acoustic post-processing of the computed unsteady flow field is often performed using the Kirchhoff method or by integration of the Ffowcs Williams - Hawkings (FW-H) equation for a porous surface.
In the present study we use a 3-D DES code and a FW-H approach for the convective wave equation and permeable data surface that does not correspond to a physical body.[1]
The main objectives of this research are:

1. Validation of a 3-D DES code for turbulent jet simulations.
2. Development of a process chain for prediction of the far-field noise.
3. Demonstration of the validity and applicability of the 3-D DES code and the efficient coupling to a FW-H solver to the innovation of aircraft engine design processes.

In the present study we will apply the newly developed tools to investigate configurations of practical interest. The aim is to develop a robust and efficient tool chain for the industrial design of modern aircraft engines, in particular with respect to low noise design.

II. Methodology

II.A. Flow Simulation

The coupled investigation of the flow and acoustic field in a forced mixer, two conflicting requirements can be identified: Firstly, the method must be capable of simulating the inherently unsteady detached shear layer, and secondly, it must be computationally cheap enough to allow the inclusion of the core and bypass regions upstream of the mixer. A natural choice for the computation of unsteady flows would be LES, where the large, energy-bearing eddies are resolved and only the small, isotropic eddies need modeling. However, the required spatial and temporal resolutions are large, especially in the attached boundary layers. Therefore, a hybrid RANS/LES scheme appears to be the most promising approach to this problem. Since in this geometry the separation point is clearly defined at the mixer, Detached Eddy Simulation (DES) may be used. In the detached shear layer behind the mixer, the model runs in "LES" mode, whereas the attached regions in core and bypass as well as the centerbody and casing boundary layers are simulated in "RANS" mode. The model used for the present application is an adaptation of a "classical" DES approach to two-equation models (cf. Strelets[2]). In the model, the turbulence length scale of a RANS type eddy-viscosity model, in terms of a k-ω-model,

$$l_{k\omega} = \frac{\sqrt{k}}{\omega} \tag{1}$$

is complemented by an LES-type filter which may, essentially, be any valid LES filter. As in many cases, the mesh resolution $\Delta = \max(\Delta_i, \Delta_j, \Delta_k)$ is used as the filter width, so that the length scale of the turbulence model is replaced by

$$l = \min\left(l_{k\omega}, C_{\mathrm{DES}}\Delta\right) \tag{2}$$

The constant C_{DES} corresponds to the Smagorinsky constant of standard LES subgrid stress models. It has to be calibrated to reflect the dissipativeness of the numerical scheme used in the particular flow solver and is usually in the order $C_{\mathrm{DES}} \approx 10^{-1}$, in this case $C_{\mathrm{DES}} = 0.15$. The original model's destruction term of the k-ω turbulence model by Wilcox[3] can be rewritten as

$$\epsilon = \beta k\omega = \frac{\beta k^{\frac{3}{2}}}{l} \tag{3}$$

with l being set according to eq. (2) for DES computations and according to eq. (1) for RANS computations.

II.B. Far-Field Propagation

To compute the far-field directivity, the pressure is needed more than a few diameters from the jet, and can not be computed directly by the DES. For the evaluation of the far-field sound we use the FW-H equation. The FW-H theory[4] which generalizes Lighthill's[5] acoustic analogy was modified by Wellner.[6] Instead of using the wave equation for a medium at rest the convective wave equation was used to derive the FW-H formulation for the time-domain solution. This solution was also reformulated in the frequency-domain. Weckmüller[1] extended this integral method for unsteady harmonic CFD solutions and axisymmetrical configurations via a circumferential decomposition of the solution, to reduce the surface integral to a sum of line integrals.
Without loss of generality the system of coordinates is chosen such that $\mathbf{e_1}$ is aligned with $\mathbf{u_0}$, thus $\mathbf{u_0} = (U_0, 0, 0)$. The time-domain integral solution, using the Green function for homogeneous flow (see, e.g. Michalke and Michel[7]), is:

$$\begin{aligned} 4\pi p'(\mathbf{x},t) &= \frac{\partial}{\partial t}\int\limits_S \left[\frac{\rho_0 u_{0i} u_j' \Gamma_{1j} + (\rho_0 u_i' + \rho' u_{0i})(c_0 - u_{0j}\Gamma_{1j}) + p'\Gamma_{1i} - \tau_{ij}\Gamma_{1j}}{c_0 R_e D_f} n_i\right]_\tau dS \\ &+ \int\limits_S \left[\frac{\rho_0 u_{0i} u_j' \Gamma_{2j} - (\rho_0 u_i' + \rho' u_{0i}) u_{0j}\Gamma_{2j} + p'\Gamma_{2i} - \tau_{ij}\Gamma_{2j}}{R_e^2 D_f^2} n_i\right]_\tau dS. \end{aligned} \tag{4}$$

The source (element on the surface) is described by $(\mathbf{y}, \tau)$ with $\mathbf{y} = (y_1, y_2, y_3)$, $\tau = t - R_e/c_0$ being the retarded time. The observer is described by $(\mathbf{x}, t)$ with $\mathbf{x} = (x_1, x_2, x_3)$.
Here the volume terms are neglected. This is possible if the mean flow is assumed to be homogeneous outside the source volume and can be done without loss of accuracy while affording a greater numerical efficiency.
In this study we restrict ourselves to the time-domain formulation of the FW-H equation (eq. 4). The frequency-domain formulation and the reduction to line integration can be found in Weckmüller.[1]

III. Numerical Methods

III.A. Flow Solver

The computations have been carried out using the CFD solver *TRACE*(Turbomachinery Research Aerodynamic Computational Environment).[8,9] *TRACE* has been designed at the Institute of Propulsion Technology specifically for turbomachinery applications, and is established as DLR's standard CFD solver for internal flows. In the default configuration, the code solves the Reynolds-averaged Navier-Stokes equations on structured and unstructured multi-block curvilinear meshes using the finite volume method.

Convective fluxes of the RANS equations are discretized using the TVD (total variation diminishing) upwind scheme by Roe; for viscous fluxes central differences are used. For time integration a third-order accurate implicit numerical scheme is used.[8] Non-matching interfaces, like adjacent blade rows or the flow downstream of the lobed mixer, are coupled using a conservative zonal approach.[10,11]

Turbulence modeling is based on the k-ω-model by Wilcox.[3] Several modifications to account for the effects of compressibility and streamline curvature have been implemented as well as a fix for spurious production of turbulent kinetic energy in stagnation regions.[12] However, these extensions have been disabled in the present study. For investigations like the present one, the model has been extended by a DES scheme for two-equation models based on a classical DES approach by Strelets.[2] In detached flow regions, a smooth blending from the upwind scheme to a central differencing scheme takes place as the turbulence model switches from RANS to LES mode. Switching is carried out using the so-called "DES ratio", i.e. the ratio of DES and RANS length scales:

$$o_{\mathrm{DES}} = e^{-\frac{1}{c_b}\frac{l_{\mathrm{DES}}}{l_{k\omega}}}. \tag{5}$$

Thus, with $l_{\mathrm{DES}} \gg l_{k\omega}$, $o_{\mathrm{DES}} \to 0$, whereas for $l_{k\omega} \gg l_{\mathrm{DES}}$, $o_{\mathrm{DES}} \to 1$. Increasing the value of the constant c_b increases the central bias of the scheme. The blending o_{DES} is then added to the MUSCL schemes parameter κ,[13] so that, e.g. for the cell interface with index $i+\frac{1}{2}$, the left and right side values of a transported property

ϕ are

$$\phi^L_{i+\frac{1}{2}} = \phi_i + \frac{1}{4}\left[(1-\kappa+o_{\mathrm{DES}})(\phi_i-\phi_{i-1}) + (1+\kappa+o_{\mathrm{DES}})(\phi_{i+1}-\phi_i)\right] \quad (6)$$

$$\phi^R_{i+\frac{1}{2}} = \phi_{i+1} - \frac{1}{4}\left[(1+\kappa+o_{\mathrm{DES}})(\phi_{i+1}-\phi_i) + (1-\kappa+o_{\mathrm{DES}})(\phi_{i+2}-\phi_{i+1})\right]. \quad (7)$$

Note that, in the present investigation, $\kappa = 0$, so that $0 < o_{\mathrm{DES}} < 1$ is sufficient for blending between upwind and central schemes. For different values of κ, the range of o_{DES} needs to be adjusted as well to correspond to the range between the upwind value and $\kappa + o_{\mathrm{DES}} = 1$. This way, the inherent stability of a second order upwind scheme is kept in RANS regions, whereas in regions where the model functions in LES mode, the damping is reduced in comparison to the standard upwind scheme. In the present study, the bias constant was set to $c_b = 5.0$.

III.B. Computational Setup

The complex geometry of the selected case lobed mixer containing 14 segments can be seen in figure 1. During the generation of the CFD mesh, care has to be taken that acoustic waves are sufficiently resolved to propagate in any direction, independent of local flow conditions. Therefore, the mesh was build in such a way, for the fluid at rest, at least approximately 80 points per wave length λ_0 of a pressure wave at the characteristic frequency f_0 for free-field conditions were available. In the worst case, i.e. an upstream-travelling wave in the bypass, more than 40 nodes per wave length were retained. The mesh was considerably refined in the boundary layers, in wall-normal direction, care was taken to ensure that $y^+ \approx 5$ for all boundaries. A continously formulated wall function[14] was used to ensure that a correct boundary layer velocity profile was enforced, the turbulence model boundary conditions were correspondingly modified to allow a smooth transition between sublayer and log layer profiles. In the shear layers, the mesh refinement that emanates from the boundary layers is retained. Furthermore, the mesh has been refined in axial and lateral directions to allow the DES model to switch to LES mode in this region. In total, the computational mesh contained approximately 40 million points for the one segment of the mixer that was simulated. One period of frequency f_0 was resolved with 512 time steps, 32 of which were recorded for later analysis. The computation was initialized from a steady-state RANS computation. Before data recording started, a sufficient period, approximately 60 periods based on frequency f_0, had to be waited to allow unsteady structures to develop in the shear layers. In total, 3-D field data were recorded for four periods, whereas 2-D data were recorded for 11 periods.

The high spatial resolution of the DES requires a large amount of disk space to save the entire 3-D flow field over a time period sufficient for data analysis. Therfore, in this work a pre-processing tool[15] has been used to define analysis surfaces for to be used with the FW-H propagation code.
The idea behind an analysis surface is a tool which is able to create user-defined surfaces in the simulation domain for the post-processing. This tool makes use of the libraries provided by the *Visualization Toolkit*[16] by *Kitware*. It is a software system for 3-D computer graphics, image processing and visualization that is being used in *Paraview* in the first place.
A new user-defined variable is assigned to each single point of the 3-D mesh. By means of a contour filter a iso-contour surface at a constant value can be created. Its numerical method equals the creation of an iso-contour surface of for example vorticity. As a result an axisymmetric surface is obtained with an unstructured topology. The elements of the mesh have the characteristic trait of being in exactly one 3-D element. These elements are shown in figure 2. The same method is also applicable to hybrid mesh topologies. The whole surface is also block structured in the same way the surrounding 3-D blocks are. That way every 3-D block has only to deal with a part of the surface associated with it.
This facts simplify and accelerate the necessary algorithm for interpolation from the 3-D flow field to the new surface.
In figure 3 one possible definition of a iso-contour definition to create an open FW-H surface is shown.
Additionally, it is possible to organize the elements into a band structure with the help of the same contour filter. This allows a circumferential decomposition of every surface to be easily performed on every position in the flow field. Moreover, this enables the transformation of Fourier data from the relative to the absolute system as well as the use of the FW-H formulation mentioned above with a sum of line integrals to speed up the computation of the far-field sound.

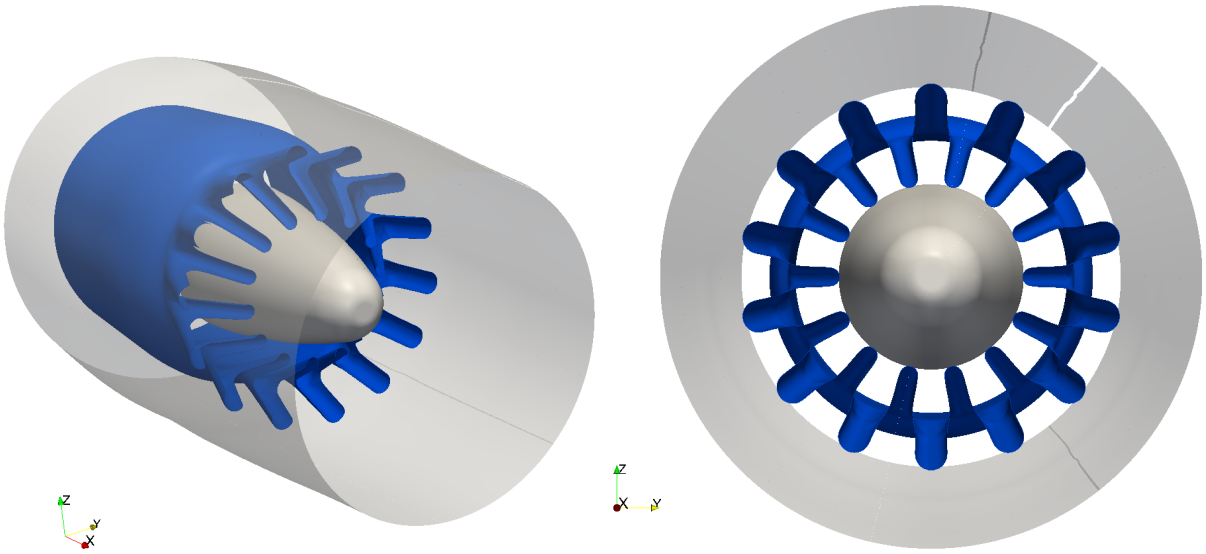

Figure 1. Geometry of the lobed mixer

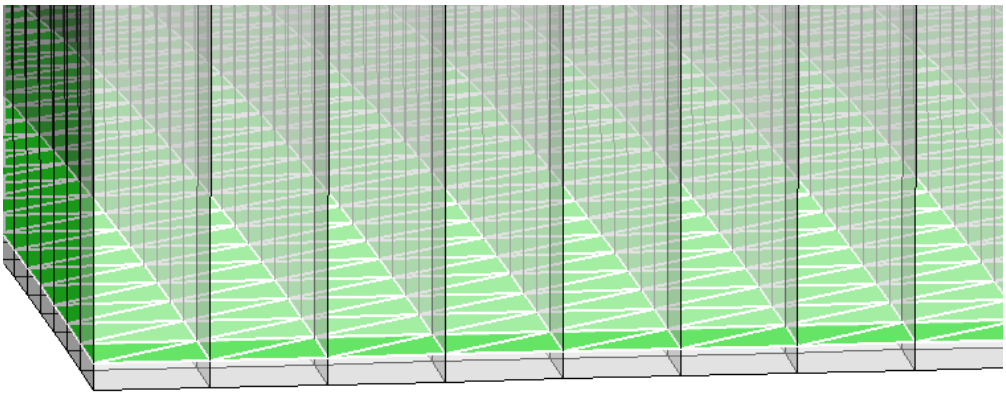

Figure 2. Elements of the created iso-surface (green) in respect to the 3-D Elements(gray)

IV. Results

IV.A. Aerodynamic calculations

The global structure of the unsteady flow, including the shear layer between core and bypass and between nozzle and exterior flow, can be seen from figure 4. Behind the mixer lobes, a complex shear layer pattern emerges, with vortical structures becoming larger as they are convected downstream from the mixer. In figures 5 and 6, the shear layers from the mixer lobes and the outer shear layer between bypass and exterior domain are shown for four different axial positions that are half a nozzle-diameter apart starting in the nozzle exit plane. On the left hand side of each picture, the vorticity is shown, representing the turbulent fluctuations that are resolved by the simulation. On the right side, the subgrid turbulent kinetic energy shows the part of the turbulent fluctuations that are modeled by the subgrid model. It is apparent that the fraction of turbulent stresses that are modelled is much greater in the outer shear layer than in the shear layer from the mixer lobes. As the vortices from the mixer are convected downstream, a more distinct pattern evolves, i.e., the vortices separate from each other and are clearly defined (cf. the left halves of the figures). At the same time, the subgrid-scale stresses diffuse in the surrounding of the vortices. Some of the subgrid stresses are dissipated, as can be seen from the absolute values of the subgrid turbulent kinetic energy in the first three axial slices. When the vortex from the upper mixer lobe touches the outer shear layer, the vortex falls apart very rapidly, as shown in the last axial slice. At this point, the most considerable

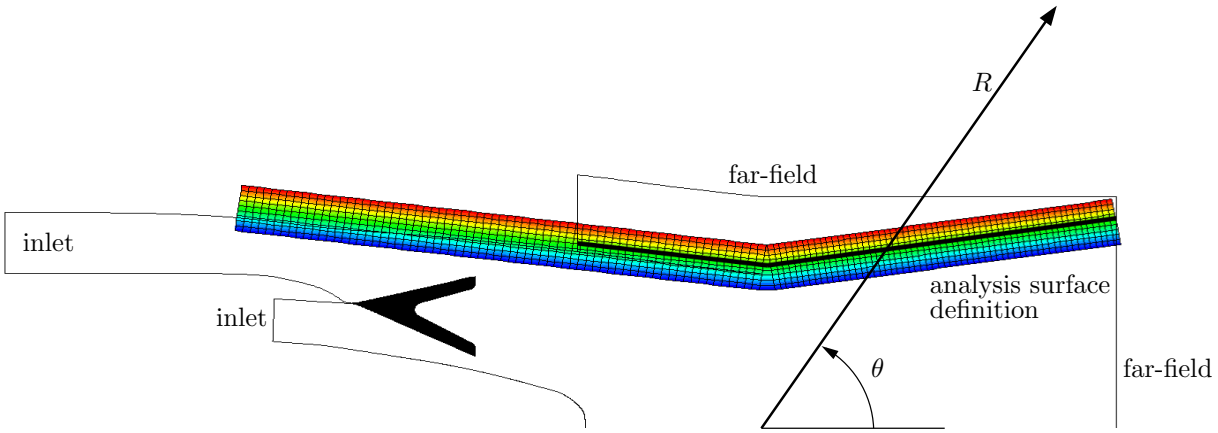

Figure 3. Schematic showing how the angle θ is measured from the jet axis, the mixer geometry. Definition of the iso-contour variable (colored) to a 3-D axisymmetrical grid and one FW-H surface (black).

amount of turbulent stresses is contained in the subgrid stresses, whereas the resolved stresses in the outer shear layer and the mixer vortices decay.

The analysis of the pressure fluctuations of frequency f_0 at different axial positions (figure 7) shows the main locations where these tones are generated. Near the vortices that are created by the mixer lobes and subsequently convected downstream, strong pressure fluctuations of this frequency can be observed, indicating that these tones are indeed generated by the shear layer interactions. In the rear part of the computational domain, where the vortex interacts with the outer shear layer, very strong fluctuations are visible.

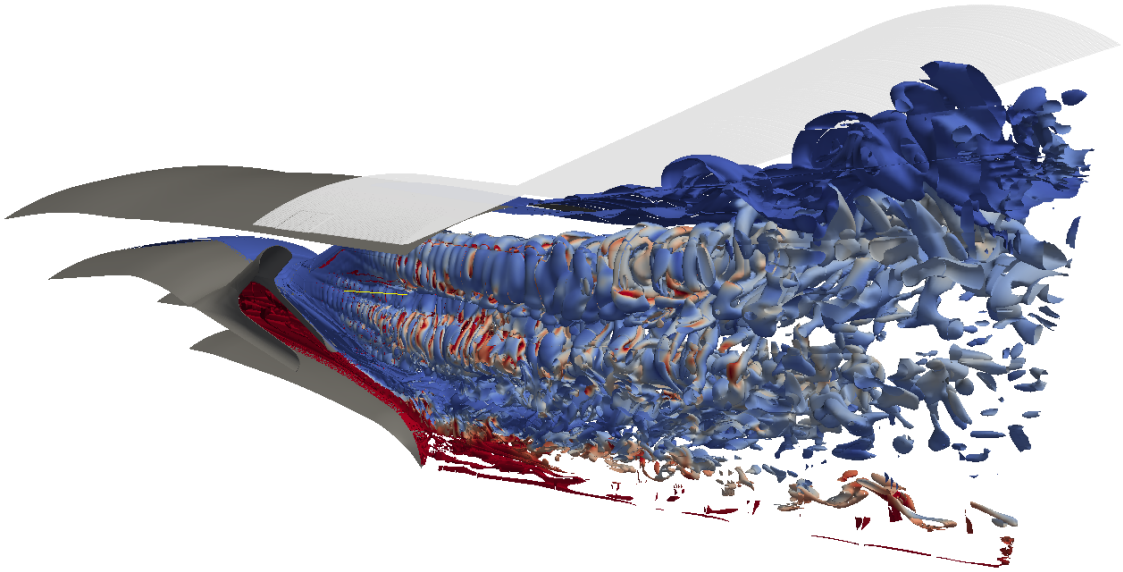

Figure 4. Iso vorticity surfaces ($\omega = 2000\ [1/s]$ and one possible permeable FW-H surface (light gray). The vorticity surface has been colored with the air temperature, from blue (cold) to red (warm) to illustrate the mixing between core and bypass flow.

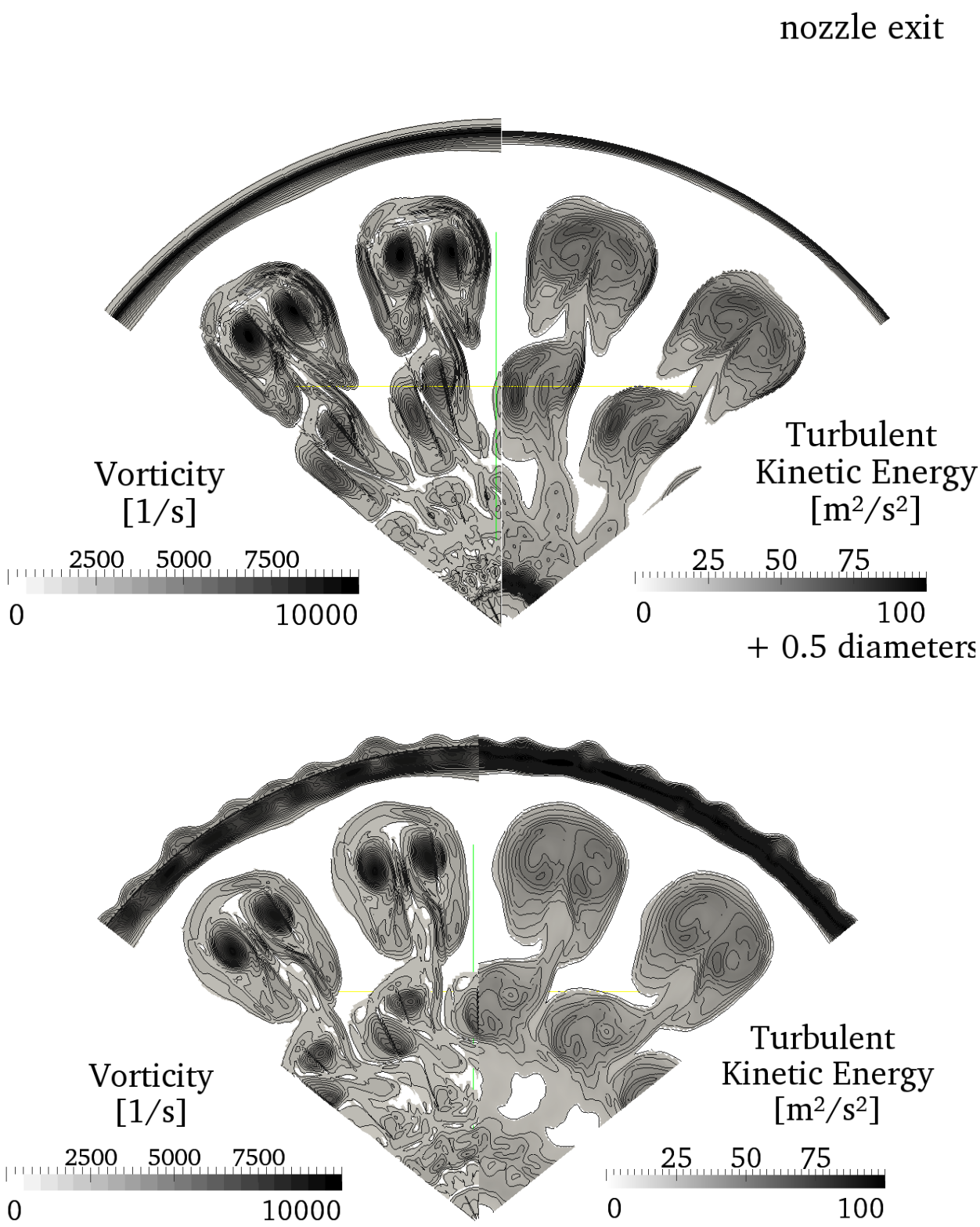

Figure 5. Vorticity magnitudes and subgrid turbulence kinetic energy at two different axial positions in the nozzle exit and half a nozzle diameter behind the exit.

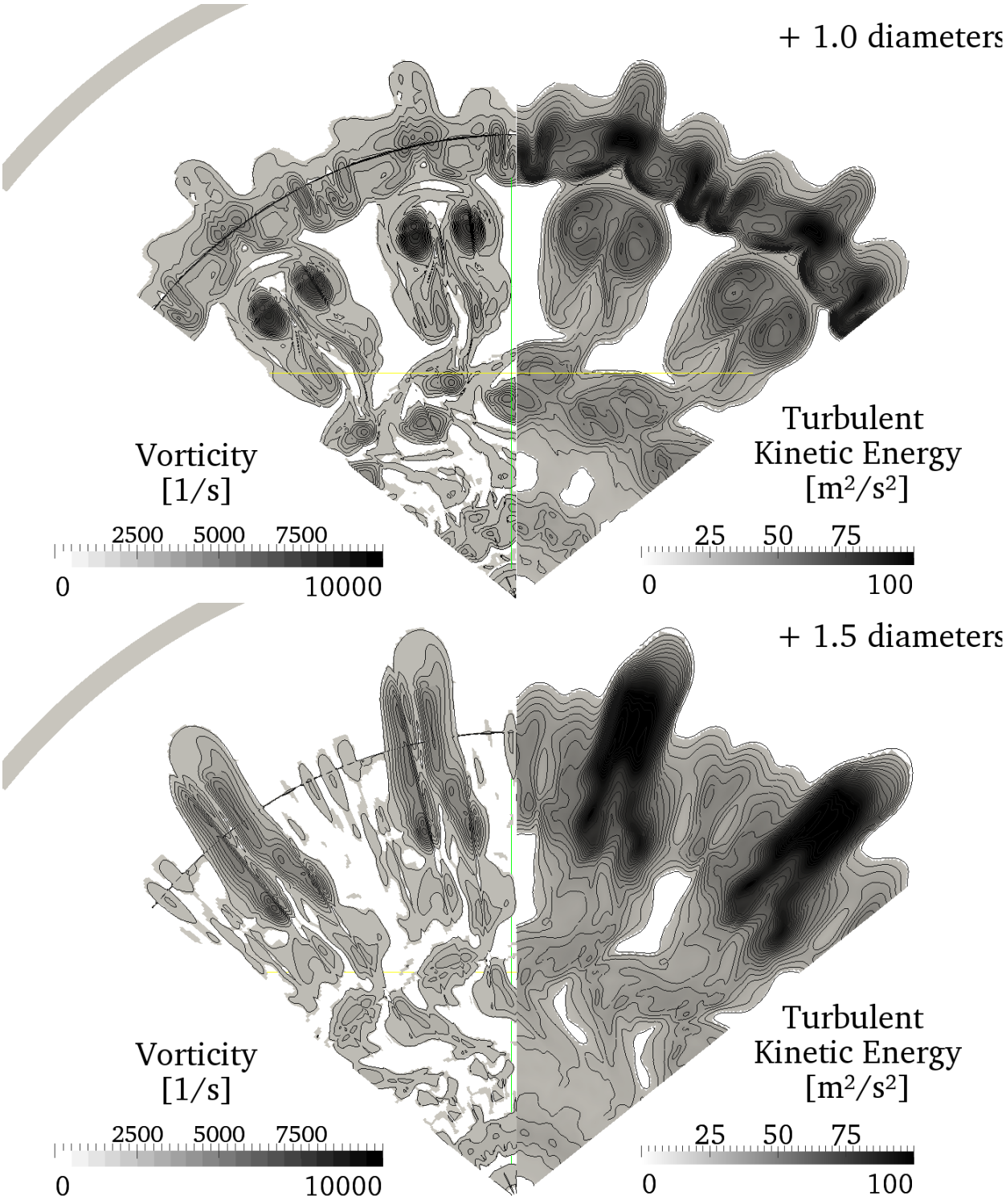

Figure 6. Vorticity magnitudes and subgrid turbulence kinetic energy at two different axial positions, one and 1.5 nozzle diameters behind the exit.

IV.B. Far-field noise computation

To investigate the far-field sound, it would be very un-economical to extend the fine-grid region of the DES far enough to determine far-field behavior. This extrapolation to large distances is done with a FW-H solver. For this reason the far-field sound is calculated using information only from the high-quality region of the

DES, and considering the outer region of the DES grid as an "extension" that places the inexact boundary conditions far enough from the turbulence, but does not support the sound waves accurately.
The exact forms of the Lighthill and FW-H formulas demand the solution over the entire space. The most typical approximate step, which is also taken here, is to neglect the external quadrupoles in the FW-H formula. Doing so the dimension of the integral is reduced from four to three. Also the usual issue with finite samples of a turbulent signal is present, namely, that Fourier series are taken of a signal that is not periodic. Then, the amplitude of the signal "discontinuity" at the ends of a sample is large. Because of the broadband nature of the acoustic source, we use the time-domain solution of the FW-H equation (eq. 4).
All these considerations lead to one porous FW-H surface (see fig. 4) placed outside of the nozzle which has no closing disk downstream. The position is near the shear layer, but far enough to have only little effects on the FW-H surface.
We can expect a high resolution of the acoustic waves for the present test since the size of the elements correlates with the resolution of the existing 3-D grid. The average size between the data points lead to 80 points per acoustic wavelength for the frequency f_0. The temporal resolution for this frequency is 32 pictures for one period. Overall 11 periods are used for the following far-field computation.
The acoustic pressure was calculated at an observer position with the help of the FW-H solver. Basically, it is possible to implement an in-depth analysis such as the entire far-field directivity of a jet. See figure 3 for the location of the observer point. The radius of the arc is equal to 60 jet radii and its center is chosen as the centerline of the jet nozzle exit as shown in figure 3. The angle θ measured form the jet axis for investigated observer position is 60°.
Figures 8 and 9 show the acoustic pressure time signal and the acoustic pressure spectra at the observer position. Fast Fourier Transform (FFT) with windowing (Hamming) was applied to the time signal to get the acoustic pressure spectra. This was done in order to smooth the spectra.
The maximum of the acoustic energy can be found in frequencies below the frequency f_0. So, the assumption about the spatial resolution of the FW-H surface is justified to resolve the acoustic waves well.
The results obtained using this method are within the expected range,[17] but unfortunately cannot be validated against measurements for this particular test case, yet.
The sources region of the the predominat low frequencies in the far-field can be found where the shear layers interact with each other; as observed in figures 10 and 11. The corresponding pressure history and sound pressure level, recorded on a FW-H surface positioned right above this area are shown in figures 12 and 13.

V. Conclusion

Using state-of-the-art numerical techniques, a Computational Aeroacoustics (CAA) methodology for jet noise prediction was applied and tested. The CAA methodology has three main components. The first one is a 3-D Detached Eddy Simulation (DES) code. This DES code employs low dispersion second order upwind scheme in DES regions and the standard MUSCL scheme in RANS regions. Time integration is accomplished by means of a 3rd-order, 4-stage implicit Runge-Kutta method. The secound component is a general and flexible coupling to a far-field propagation code. The third component of the CAA methodology consists of integral acoustics methods. We have applied an acoustic code that employs the Ffowcs Williams - Hawkings (FW-H) surface integral method.
The flow solution using a turbomachinery CFD solver and a DES model for turbulence modeling shows good results. Turbulent fluctuations were found to develop very quickly in flow regions where enhanced turbulence is expected, i.e. the shear layers behind the mixer lobes. A great part of the turbulent fluctuations in these regions could be directly resolved, while the outer shear layer between the bypass and the exterior computational domain contained a great deal of subgrid turbulent stresses. When the main vortices behind the mixer lobes started passing through the outer shear layer, ca. 1.5 nozzle diameters downstream of the nozzle exit, they broke up very quickly as they were convected further downstream. Also, from this point on, a considerable amount of the turbulent stresses was found to be contained in the subgrid stresses while the resolved stresses decayed very quickly (and dissipated into subgrid stresses).
The predominant low frequencies can be found in regions where the shear layers interact with each other.
With the help of our pre-processing tool we are able to place data surfaces in every region in the flow-field. It is shown that the spatial as well as the temporal resolution of the mesh are adequate to capture and analyse acoustic waves at the dominant frequencies.
The predicted far-field noise levels and spectrum using the FW-H approach display the expected tendencies.

The next step is a deeper investigation of the acoustic field and physical mechanism of the noise generation. This will be done by MTU Aero Engines GmbH in the context of the MASSIF-EffekT project. It will also give some general guidelines for reliable acoustic analysis of any jet aerodynamic simulation using the FW-H surface integral method.

Acknowledgment

This work has been carried out in the context of the MASSIF-EffekT project in cooperation with MTU Aero Engines GmbH. The authors also thank Dr. Sebastien Guérin and Christian Weckmüller for providing the FW-H solver used in this work.

References

[1]Weckmüller, C., Guérin, S., Wellner, J., and Michel, U., "Ffowcs Williams & Hawkings Formulation for the Convective Wave Equation and Permeable Data Surface," *Proceedings of the 16th AIAA/CEAS-Aeroacoustics Conference*, Stockholm, Sweden, June 7-9 2010, AIAA Paper 2010-3710.

[2]Strelets, M., "Detached Eddy Simulations of Massively Separated Flows," *Proc. 39th Aerospace Science Meeting and Exhibit*, Reno, USA, 2001, AIAA Paper 2001-0879.

[3]Wilcox, D. C., "Reassessment of the Scale-Determining Equation for Advanced Turbulence Models," *AIAA Journal*, Vol. 26, No. 9, 1988, pp. 1299 – 1310.

[4]Ffowcs Williams, J. E. and Hawkings, D. I., "Sound Generation by Turbulence and Surfaces in Arbitrary Motion," *Philosophical Transactions of the Royal Society*, Vol. 264, No. A 1151, Mai 1969, pp. 321–342.

[5]Lighthill, M. J., "On Sound Generated Aerodynamically I: General Theory," *Proceedings of the Royal Society*, Vol. 211, London, 1952, pp. 564–587.

[6]Wellner, J., *Herleitung und Anwendung der konvektiven Kirchhoff-Ffowcs-Williams-Hawkings-Gleichung*, Master's thesis, Technische Universität Berlin, Müller-Breslau-Str. 8, 10623 Berlin, Deutschland, May 2009.

[7]Michalke, A. and Michel, U., "Prediction of jet noise in flight from static tests," *Journal of Sound and Vibration*, Vol. 67, No. 3, March 1979, pp. 341–367.

[8]Ashcroft, G., Heitkamp, K., and Kügeler, E., "High-order accurate implicit runge-kutta schemes for the simulation of unsteady flow phenomena in turbomachinery," *Proceedings of V European Conference on Computational Fluid Dynamics ECCOMAS CFD*, Lisbon, Portugal, 2010.

[9]Becker, K., Heitkamp, K., and Kügeler, E., "Recent progress in a hybrid-grid cfd solver for turbomachinery flows," *Proceedings of V European Conference on Computational Fluid Dynamics ECCOMAS CFD*, Lisbon, Portugal, 2010.

[10]Yang, H., Nürnberger, D., Nicke, E., and Weber, A., "Numerical Investigation of Casing Treatment Mechanisms with a Conservative Mixed-Cell Approach," *ASME IGTI*, 2003, Paper-No. 2003-GT-38483.

[11]Yang, H., Röber, T., and Kozulovic, D., "Hybrid-Grid Simulation of Unsteady Wake-Boundary Layer Interaction on a High Lift Low Pressure Turbine Airfoil," *Proceedings of GT2007: ASME Turbo Expo 2007: Power for Land, Sea and Air*, Montreal, Canada, May 2007.

[12]Franke, M., Röber, T., Kügeler, E., and Ashcroft, G., "Turbulence Treatment in Steady and Unsteady Turbomachinery Flows," *Proceedings of the V European Conference on Computational Fluid Dynamics ECCOMAS CFD 2010*, Lisbon, Portugal, June 2010.

[13]Hirsch, C., *Numerical Computation of Internal and External Flows – Computational Methods for Inviscid and Viscous Flows*, Vol. 2, Wiley, 1st ed., 1990.

[14]Spalding, D. B., "A Single Formula for the "Law of the Wall"," *Journal of Applied Mechanics*, Vol. 28, 09 1961, pp. 455–458.

[15]Voigt, C., Frey, C., and Kesken, H.-P., "Development of a Generic Surface Mapping Algorithm for Fluid-Structure-Intersction Simulations in Turbomchinery," *Proceedings of the V European Conference on Computational Fluid Dynamics ECCOMAS CFD 2010*, Lisbon, Portugal, June 14-17 2010, ECCOMAS Paper 2010-01737.

[16]Schroeder, W. J., Bertel, F., Malaterre, M., Thompson, D., Pebay, P. P., O'Bara, R., and Tendulkar, S., "Framework for Visualizing Higher-Order Basis Functions," .

[17]Uzun, A., Lyrintzis, A. S., and Blaisdell, G. A., "Coupling of integral acoustics methods with LES for jet noise prediction," *International Journal of Aeroacoustics*, Vol. 3, No. 4, 2005, pp. 297–346.

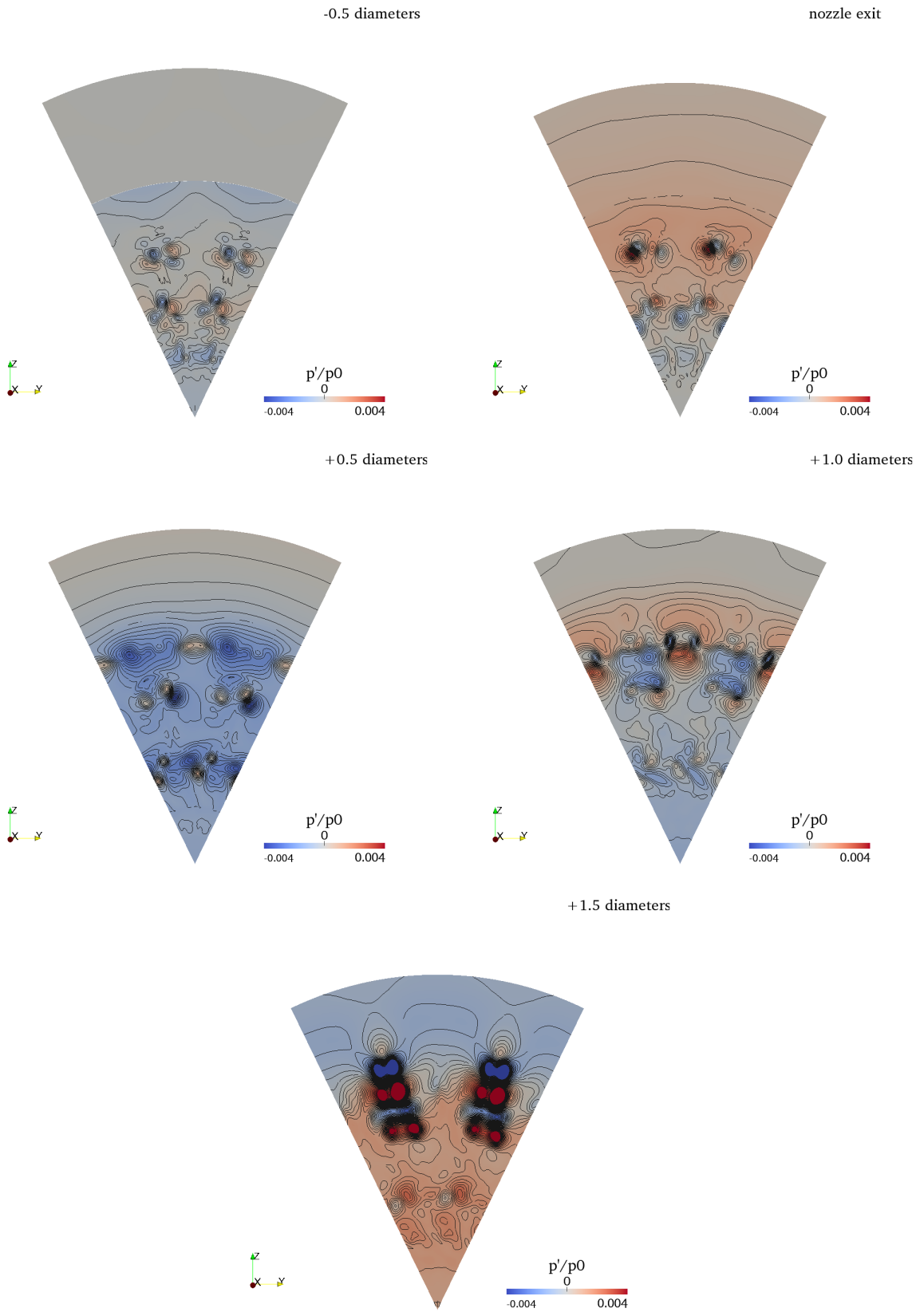

Figure 7. Real part of the pressure fluctuations at f_0 for five axial positions, from 0.5 nozzle diameters inside the nozzle to 1.5 diameters downstream.

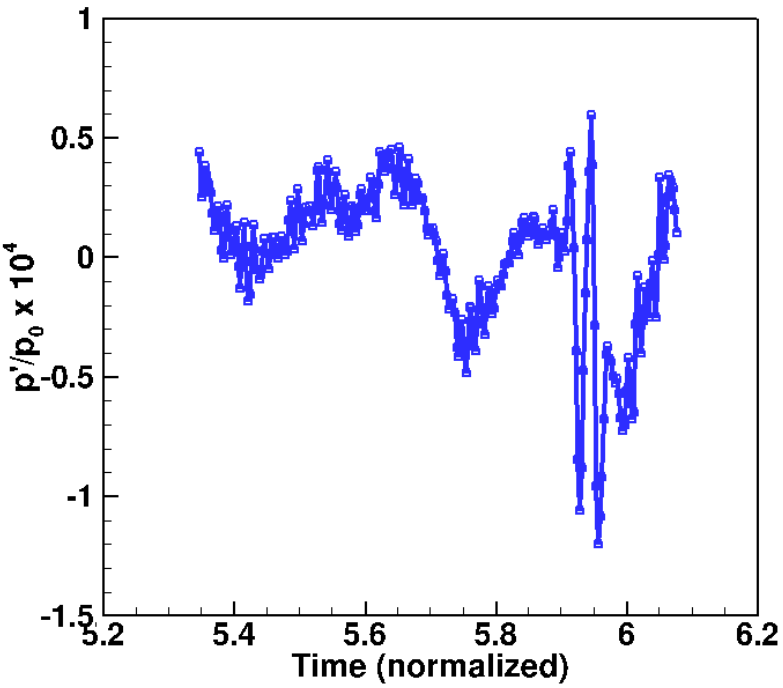

Figure 8. Pressure history at observer position $R = 60r_0, \theta = 60°$location on the far-field arc.

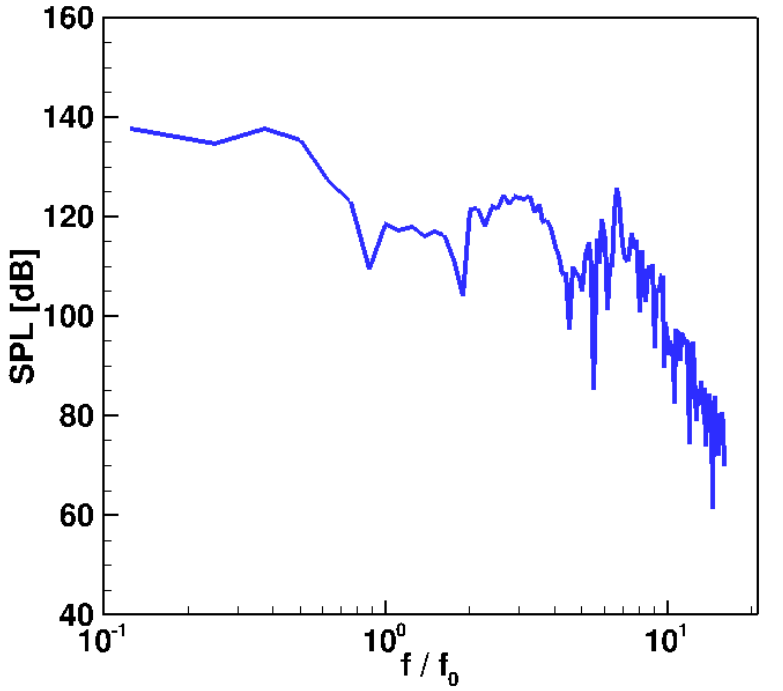

Figure 9. Sound pressure level at observer position $R = 60r_0, \theta = 60°$location on the far-field arc; bandwidth 125 Hz; windowing with Hamming function

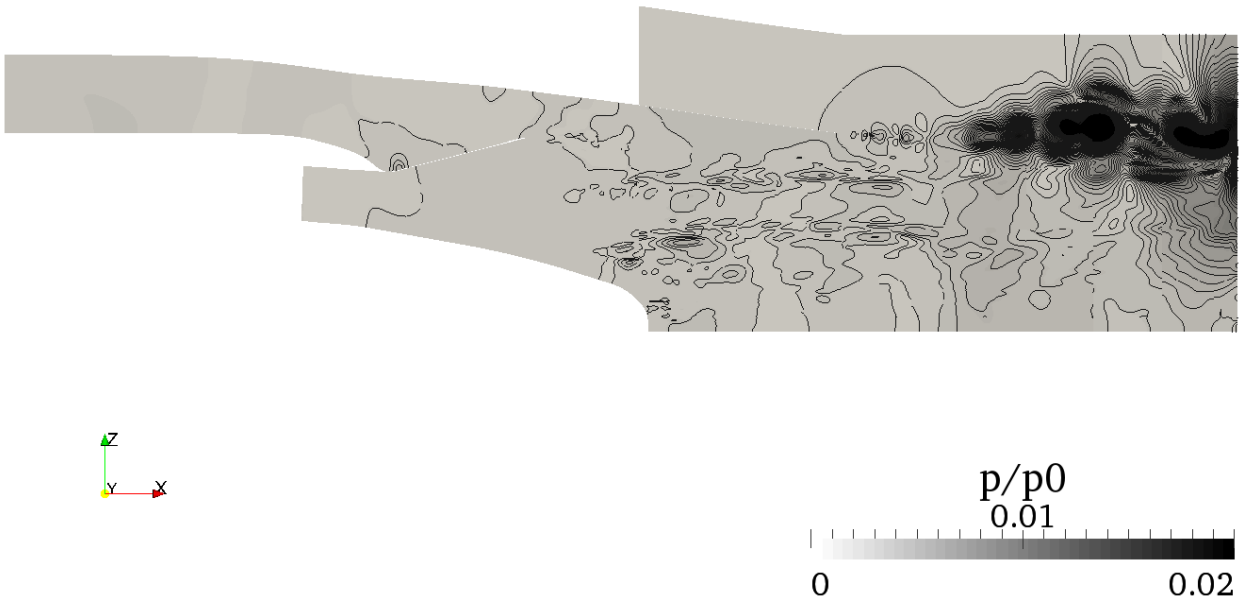

Figure 10. Pressure magnitude at f_0 for one radial position

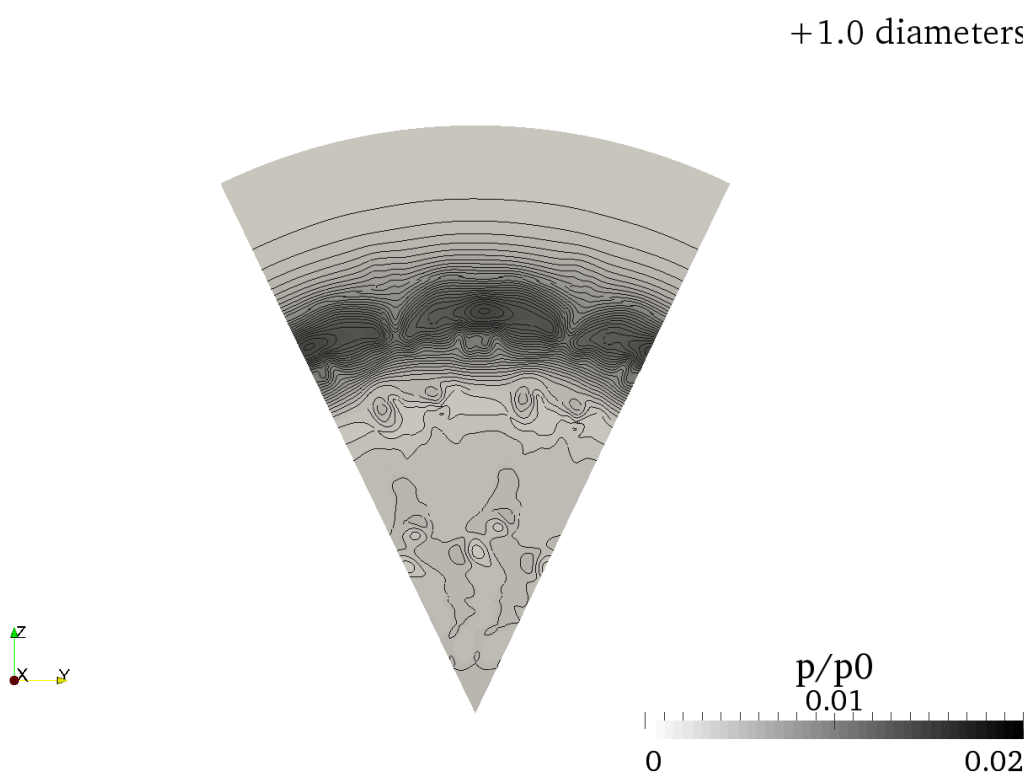

Figure 11. Pressure magnitude at f_0 for the axial posion 1 nozzle diameter downstream.

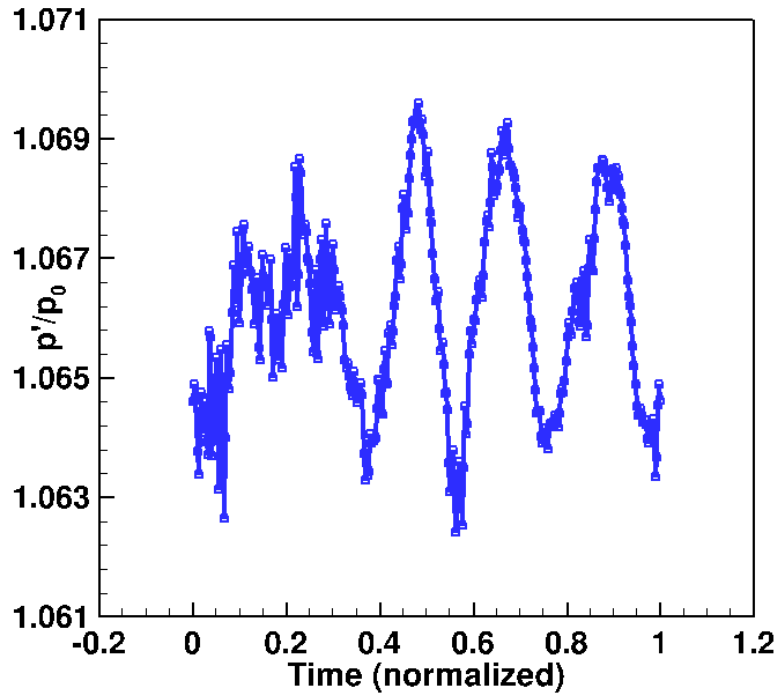

Figure 12. Pressure history at $R = 1.3r_0, \theta = 60°$on FW-H surface

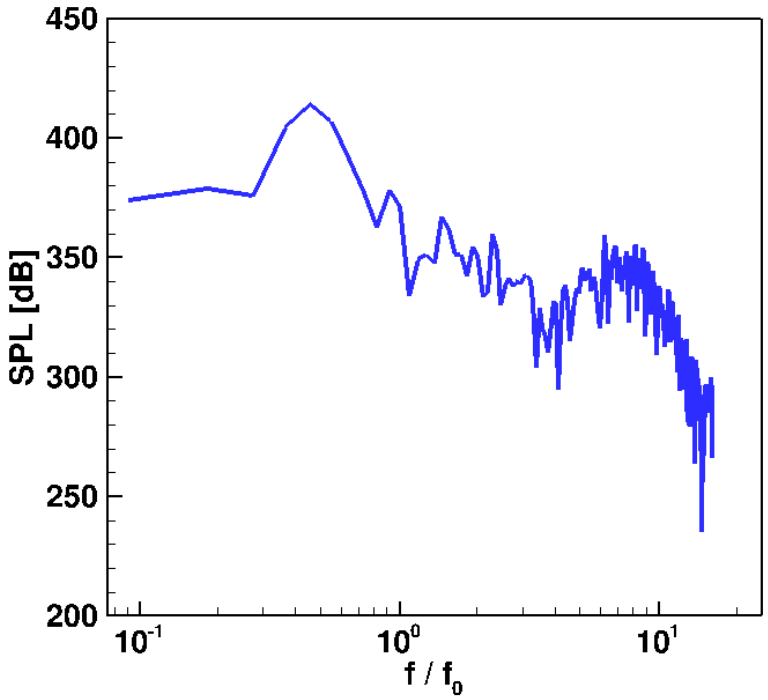

Figure 13. Sound pressure level at $R = 1.3r_0, \theta = 60°$on FW-H surface; bandwidth 90 Hz; windowing with Hamming function